Effects of Nucleotides on the Protein Ligands to Metals at the M2 and M3 Metal-Binding Sites of the Spinach Chloroplast F_1-ATPase†

Andrew L. P. Houseman,‡ Russell LoBrutto, and Wayne D. Frasch*

The Center for the Study of Early Events in Photosynthesis, Department of Botany, Arizona State University, Tempe, Arizona 85287-1601

Received December 8, 1994⊗

ABSTRACT: We have identified the most probable protein ligands at the catalytic M3 and noncatalytic M2 metal-binding sites in the spinach chloroplast F_1-ATPase (CF_1) and here propose possible residues in the protein sequence for these ligands in latent CF_1 in the absence of nucleotide. The changes in the metal ligands at these sites upon binding of nucleotide to the N2 and N3 sites and upon activation of latent CF_1 provide a possible molecular basis for inhibition of ATPase activity by free metal, for the lack of activity in the latent state, and for the gating mechanism of the ATPase H^+ pump. To these ends, the Mg^{2+} analogue, vanadyl $(V^{IV}{=}O)^{2+}$, was used as a paramagnetic probe at the M2 and M3 metal-binding sites. EPR and ESEEM spectra of VO^{2+} were obtained, and simulations of the full EPR spectra imply the ligand sets at the different metal-binding sites. When VO^{2+} is added to CF_1 in the absence of ATP, the most likely set of ligands at the M2 site are 1 ROH (αT176), 2 H_2O, and 1 $RCOO^-$ (αD269 or αD270), where the suggested amino acid designations of the residues are given in parentheses according to the mitochondrial sequence. Evidence suggests a possible axial nitrogen ligand at this site (αK175). When the M2 site is filled by addition of VO^{2+} and ATP, the metal binds as a second species in which N2-bound ATP and M2-bound VO^{2+} form a monodentate complex with concomitant exchange of the equatorial protein ligands by 3 H_2O. The M3 sites also exists in two forms: (i) in latent CF_1, the data are best fit with 1 ROH (βT163), 1 $RCOO^-$ (βD256 or βE188), and 2 H_2O as ligands; and (ii) after the ATPase has been activated, the two phosphates of the ADP bound to the N3 site may coordinate to the metal bound to the M3 site. The best fit of the coordination sphere for this second form of M3-bound VO^{2+} is 2 ROH (βT163 and αS344) and 2 phosphates (from ADP). Evidence suggests that there is an axial nitrogen ligand at this site (βK162) and/or the M2 site (αK175). The determination of metal ligands provided by this and earlier studies with vanadyl permits a correlation between the sites of the crystal structure and the order of filling: N1, N2, N3, etc.

The chloroplast F_1-ATPase (CF_1)[1] is the extrinsic membrane protein complex that, in association with the intrinsic membrane complex F_0, couples the protonmotive force generated by the light reactions of photosynthesis to synthesize ATP. CF_1 has a subunit stoichiometry of $\alpha_3\beta_3\gamma\delta\epsilon$ of which the α and β subunits have significant sequence homology. There are three catalytic sites which, in the 2.8 Å crystal structure of the F_1-ATPase from bovine mitochondria, are primarily associated with the β subunits, each with different binding specificites so that the three sites in the crystal structure were empty or filled with an ATP analogue or ADP and were labeled β_E, β_{TP}, and β_{DP}, respectively (Abrahams et al., 1994). The ATPase activity of purified CF_1 is latent but can be activated by any of a variety of treatments. Three noncatalytic nucleotide-binding sites are also present which are primarily associated with each α subunit, but are closer to one neighboring β subunit than the other and are labeled α_E, α_{TP}, and α_{DP}, accordingly. The function of the noncatalytic sites is not known but has been suggested to be involved in modulating the activity of the catalytic sites [cf. Frasch (1994) for review].

Because of the unique binding properties that enable them to be filled selectively (Bruist & Hammes, 1981; Shapiro & McCarty, 1991), the six nucleotide-binding sites on CF_1 are designated N1 to N6. In the absence of nucleotides CF_1 has been estimated to have six binding sites for divalent metal cations as well (Hochman & Carmeli, 1985). Three of these sites, M1, M2, and M3, can be identified due to their particular binding properties (Haddy et al., 1985). Use of ammonium sulfate precipitation and chromatography results in metal-nucleotide-depleted CF_1 (mnd-CF_1) which lacks metals in all but the M1 site (Houseman et al., 1994a) and contains only one nucleotide (ADP) at the N1 site (Bruist & Hammes, 1981).

† This work was supported by grants from the U.S. Department of Agriculture (NRIC Grant 92-01249) and the H. Frasch Foundation (Grant 0188HF) to W.D.F. This is Publication No. 221 of The Center for the Study of Early Events in Photosynthesis.

* Author to whom correspondence should be addressed.

‡ ASU Center for the Study of Early Events in Photosynthesis Postdoctoral Research Fellow.

⊗ Abstract published in *Advance ACS Abstracts,* February 15, 1995.

[1] Abbreviations: AdoMet, *S*-adenosylmethionine; CF_1, soluble chloroplast F_1-ATPase; CW-EPR, continuous-wave electron paramagnetic resonance spectroscopy; DCCD, dicyclohexylcarbodiimide; DTT, dithiothreitol; ESEEM, electron spin-echo envelope modulation; HEPES, *N*-(2-hydroxyethyl)piperazine-*N*′-(2-ethanesulfonic acid); M1, metal-binding site with highest affinity; M2 and M3, cooperatively binding high-affinity metal sites; MF_1, mitochondrial F_1-ATPase; mnd-CF_1, metal-nucleotide-depleted CF_1 which contains Mg^{2+} and ADP only at site 1; N1, nondissociable catalytic nucleotide-binding site; N2, metal-ATP specific site dissociable only upon precipitation in $(NH_4)_2SO_4$ and EDTA [(ethylenedinitrilo)tetraacetate]; N3, most tightly bound dissociable catalytic site; P_i, inorganic phosphate; TNP-ATP, 2′-*O*-tetranitrophenyl-ATP; α_{DP}, β_{DP}, β_E, and β_{TP}, nucleotide-binding sites specified by Abrahams et al. (1994).

0006-2960/95/0434-3277$09.00/0

Nucleotide sites N1, N3, and N4 are believed to be catalytic while N2, N5, and N6 are noncatalytic. In the activated state, the catalytic sites bind ADP and ATP as bidentate and tridentate complexes with Mg^{2+}, respectively (Frasch & Selman, 1982; Carmeli et al., 1989; Devlin & Grisham, 1990), but are not coordinated when the enzyme is latent (Carmeli et al., 1986; Houseman et al., 1994b). In the absence of nucleotides, latent mnd-CF_1 cooperatively binds metals to M2 and M3 (Haddy et al., 1985; Hochman & Carmeli, 1985; Houseman et al., 1994a).

Vanadyl, $(V^{IV}O)^{2+}$, can serve as a functional metal cofactor for the ATPase reaction catalyzed by CF_1 and has been used as a paramagnetic EPR probe of the M2 and M3 binding sites (Houseman et al., 1994a,b). The M2 and M3 sites were each found to exist in two possible forms. The M2 site binds metal independently of nucleotide or can bind as a monodentate complex with ATP. The nucleotide in the complex was determined to be that which is bound to the noncatalytic N2 nucleotide-binding site, thus making a joint M2−N2 site. In the presence of ATP, the nucleotide phosphate inserts into the coordination sphere of the metal at M2. After the M2−N2 site is filled and the M3 site is depleted by chromatography, the M3 site fills with metal much as the catalytic N3 site fills with nucleotide. When VO^{2+} and ADP fill the M3 and N3 sites specifically, activation of ATPase activity with dithiothreitol and ethanol converts the M3 site to a different form consistent with a bidentate metal−nucleotide complex (Houseman et al., 1994b).

We now present an analysis of the protein ligands of VO^{2+} bound to the M2 and M3 sites in the presence of nucleotides using EPR spectral simulation and ESEEM spectroscopy. We find that when ATP is available to bind to N3, a change in protein coordination occurs on VO^{2+} at the M2 metal-binding site, so that the substitution of ATP phosphate into the coordination sphere replaces the protein ligands, resulting in the M2−N2 species. Changes in protein ligation that probably involve substitution of hydroxyl from either serine or threonine for the carboxylate of aspartate or glutamate occur at VO^{2+} in the M3 site upon activation of the enzyme. These changes have important implications concerning the molecular basis for free-metal inhibition of ATPase activity, the lack of ATPase activity in latent CF_1, and possibly the gating mechanism of the ATPase-driven proton pump.

EXPERIMENTAL PROCEDURES

Protein Purification and Sample Preparation. CF_1 was isolated as described previously (Houseman et al., 1994a). Prior to extraction of CF_1 from thylakoid membranes, these membranes were given three to four washes of 10 mM sodium pyrophosphate to remove ribulose-1,6-bisphosphate carboxylase (Rubisco). Strotmann et al. (1973) determined that a single pyrophosphate wash removes about 96% of the Rubisco present and that this enzyme could not be detected in a fourth pyrophosphate wash as determined by a sensitive enzymatic assay. Rubisco was also not evident by Coomassie-stained SDS−PAGE of the Houseman et al. (1994a,b) CF_1 preparations. Depletion of metal and nucleotide from CF_1 sites M2 to M6 and N2 to N6 was accomplished as per Houseman et al. (1994b) and Bruist and Hammes (1981), respectively, and this form of CF_1 is denoted "metal-nucleotide-depleted" CF_1 (mnd-CF_1). Fresh solutions of $VOSO_4 \cdot 3H_2O$ were prepared daily using deionized water that had been thoroughly sparged with dry N_2(g) to remove dissolved O_2. Some samples of CF_1 were activated in 50 mM DTT in the presence or absence of 20% ethanol.

EPR and ESEEM Measurements. CW-EPR experiments were carried out at X-band (9 GHz) using a Bruker 300E spectrometer and a liquid nitrogen flow cryostat operating at 100 K as described previously (Houseman et al., 1994a). Simulations of the CW-EPR spectra employed the program QPOWA (Nilges, 1979; Maurice, 1980) modified to include the effects of intrinsic line width (W_0) and line width that varies with the nuclear quantum number, m_I, due to **A**-strain (C_1), **g**-strain (C_2), and the combination of these effects (parameterized by ϵ). The theory concerning the line widths is given by Froncisz and Hyde (1980). Three-pulse (stimulated echo) ESEEM experiments were carried out at 4−12 K using a laboratory-built spectrometer (LoBrutto et al., 1986) operating over the 7−11 GHz range and an APD Cryogenics LTR flow cryostat to detect ^{14}N superhyperfine couplings to VO^{2+}.

^{51}V Hyperfine Couplings. The **A** and **g** tensors are a direct measure of the nature of the equatorial ligands in that the ^{51}V hyperfine coupling decreases in order with the following ligands to VO^{2+}−: H_2O; $RCOO^-$; R=N−R′; RNH_2; ROH; RSH (Chasteen, 1981; Holyk, 1979). The g values increase in this order. These studies provide a way to estimate hyperfine coupling for VO^{2+} with a mixed ligand environment. Each of the four equatorial ligands in complexes with a single type of ligand contributes equally to the observed ^{51}V hyperfine coupling. In a mixed ligand environment, each type of ligand still makes this fixed contribution. Hence, the expected hyperfine coupling is the average of couplings observed for uniform environments, weighted by the number of each type of ligand. The additivity relation for the parallel hyperfine coupling takes the form

$$A_{\|\mathrm{calc}} = \sum_{i=1} \frac{n_i A_{\|i}}{4} \qquad (1)$$

where i counts the different types of equatorial ligand donor groups, n_i(=1 to 4) is the number of ligands of type i, and $A_{\|i}$ is the measured coupling constant (from model studies) when all four equatorial ligand donor groups are of type i (Chasteen, 1981). Similar equations can be written for $g_\|$ and for A_{iso}.

RESULTS

The M2 and M3 metal-binding sites can be distinguished by filling these sites in latent mnd-CF_1 with VO^{2+} in the presence of ATP. Three 16-line spectra result from VO^{2+} bound in this manner. Figure 1 shows an enlargement of the $-5/2_\|$ region of the VO^{2+} spectrum that resolves the contributions from the three different VO^{2+} species present in the protein. The three species of bound VO^{2+} are labeled according to their assignments as M2−N2, M3, and M3−N3 from low to high field based on experiments that selectively filled and/or depleted VO^{2+} from the noncatalytic site 2 or the catalytic site 3 (Houseman et al., 1994b). To obtain information about the ligands to the metal, the entire spectrum of each of these three species was simulated separately using QPOWA. Each simulated spectrum was

Table 1: EPR Parameters of VO^{2+} Complexes Obtained Experimentally and by Eq 1

VO^{2+} equatorial ligands	^{31}P (MHz) $A_\perp$	^{14}N (MHz) A_0	^{51}V ($\times 10^{-4}$ cm^{-1}) $A_\parallel$	$A_\perp$	$g_\parallel$	$g_\perp$	refs
CF_1 + excess nucleotide							this work
M2−N2 species	18[a]		181.5	67.1	1.935	1.9784	
M3 species			169.1	60.4	1.947	1.9818	
M3−N3 species	20[a]		155.8	52.7, 42.7	1.954	1.980, 1.987	
AdoMet synthetase							*b*
1 RNH_2 (K),[c] 2 P_i (ATP), 1 H_2O?	21.4	4.3	175	67.6	1.94	1.97	
1 RNH_2 (K),[c] 2 P_i (PPP_i), 1 H_2O?	20.4	4.8	175	67.6	1.94	1.97	
1 RHN_2 (AdoMet), RO^-? (S or T)[c]	21.1	5.5	164	58.0	1.95	2.00	
4 H_2O			182.6		1.933		*d*
1 $RCOO^-/P_i$, 3 H_2O			179.6		1.935		*e*
2 $RCOO^-/P_i$, 2 H_2O			176.8		1.937		*e*
3 $RCOO^-/P_i$, 1 H_2O			173.8		1.939		*e*
2 oxalate, 4 $RCOO^-$			170.9		1.941		*f*
1 RNH_2, 2 $RCOO^-$, 1 H_2O			171.6		1.9525		*e*
1 ROH, 1 $RCOO^-$, 2 H_2O			169.35		1.9435		*e*
1 ROH, 3 $RCOO^-/P_i$			163.5		1.9475		*e*
2 ROH, 2 $RCOO^-/P_i$			156.1		1.954		*f*

[a] Houseman et al., 1994b. [b] Zhang et al., 1993; Markham, 1984. [c] Refers to the single-letter abbreviation of the amino acid side chain. [d] Albanese & Chasteen, 1978a,b. [e] Derived from eq 1. [f] Holyk, 1979.

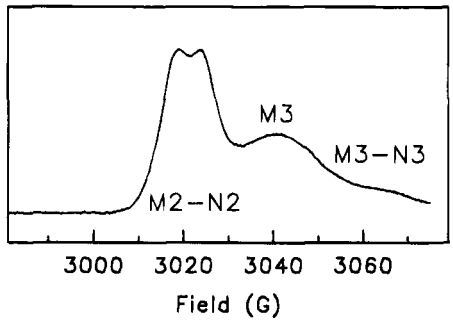

FIGURE 1: EPR spectrum of mnd-CF_1 in the presence of 3 ATP/VO^{2+} showing only the $-5/2_\parallel$ region. To 153 mg of CF_1 was added 0.67 equiv of VO^{2+} at a total volume of 255 μL. The experimental spectrum was taken at 100 K, 9.5563 GHz, 2.5-mW microwave power, 5 G modulation amplitude, 100-kHz modulation frequency, 328-ms time constant, and sweep rate 9.52 G/s.

used to determine the spin Hamiltonian parameters, and the resulting **g** and **A** tensors are listed in Table 1.

The M3 site can be filled uniquely with VO^{2+} by adding VO^{2+}-ADP to latent mnd-CF_1, which has first been treated to contain the EPR-silent Mg^{2+}-ATP at the M2−N2 site (Houseman et al., 1994b). This selective filling results in EPR signals that arise from VO^{2+} bound predominantly as the M3 species with a small proportion of M3−N3 also present (Figure 2a). The use of ADP is an additional precaution to prevent VO^{2+}-nucleotide from entering M2−N2, which is specific for ATP (Bruist & Hammes, 1981). A simulation of the entire EPR spectrum of the M3 species is shown in Figure 2c, and the spin Hamiltonian parameters are listed in Table 1.

The Mg^{2+} at the M1 site is not displaced by VO^{2+} under these conditions (Houseman et al., 1994a), nor does VO^{2+}−ADP enter other sites besides M3−N3. Furthermore, when CF_1 samples are preloaded with VO^{2+} and ATP, ammonium sulfate precipitation leaves less than 0.05 equiv of V as detected by atomic absorption spectroscopy (Houseman et al., 1994a). Thus, if VO^{2+} is capable of displacing Mg^{2+} in the M1 site of latent enzyme, very little such displacement occurs under these conditions.

Activation of CF_1 by addition of 50 mM dithiothreitol (DTT) and 20% ethanol produces a change in the EPR spectrum of VO^{2+} at the M3 site (Houseman et al., 1994b). In Figure 2d, activation by DTT alone also quantitatively converts the predominant form of VO^{2+} bound as M3 to the M3−N3 form within 5 min at room temperature, indicating a significant change in ligation to VO^{2+} at the M3 site. No further changes were observed in the EPR spectrum after the activation treatment was continued for 18 h at room temperature. The presence or absence of ethanol during the 18 h activation also did not affect the EPR spectrum compared to that shown in Figure 2d.

Figure 2f shows a control that contained the same amounts of VO^{2+}, ADP, and DTT in the absence of protein. The VO^{2+}−DTT complex produced under these conditions is only evident as a much broader central peak ($-1/2_{\parallel,\perp}$) with a peak-to-peak height that was 10% the height of the M3−N3 species. This EPR signal also implies that DTT has lower affinity for VO^{2+} than does CF_1 and cannot strip CF_1 of VO^{2+} (Houseman et al., 1994b). Room temperature EPR spectra [cf. Chasteen (1981)] confirmed that no small, EPR-visible VO^{2+} complexes were present (data not shown). Therefore, the change in the EPR signal of VO^{2+} bound to the M3 site of CF_1 upon activation is appropriately attributed to M3−N3, not to a VO^{2+}−DTT complex in solution.

The simulated EPR spectrum of the M3−N3 species observed with activated CF_1 is shown in Figure 2e, and the spin Hamiltonian parameters are summarized in Table 1. The simulation displays very weak intensity at the outside features (e.g., $\pm 7/2_\parallel$, $\pm 5/2_\parallel$) but much greater intensity at the central peak ($-1/2_{\parallel,\perp}$) compared to the EPR spectra of the other species of bound VO^{2+} examined. These effects result from the greater line width of the outside features and the significantly narrower line width of the central peak than that observed for the other species.

No differences could be distinguished between the spectrum attributed to M3−N3 in Figure 2e and that in Figure 2a. As a result, the spin Hamiltonian parameters obtained from the simulated spectra of the M3 and M3−N3 species were used to reconstruct the simulation of the experimental spectrum of Figure 2a. This simulated spectrum, shown in Figure 2b, matched the experimental spectrum reasonably well when a 3:1 ratio of integrated M3 and M3−N3 EPR intensities was used. This indicates that filling site 3 of latent

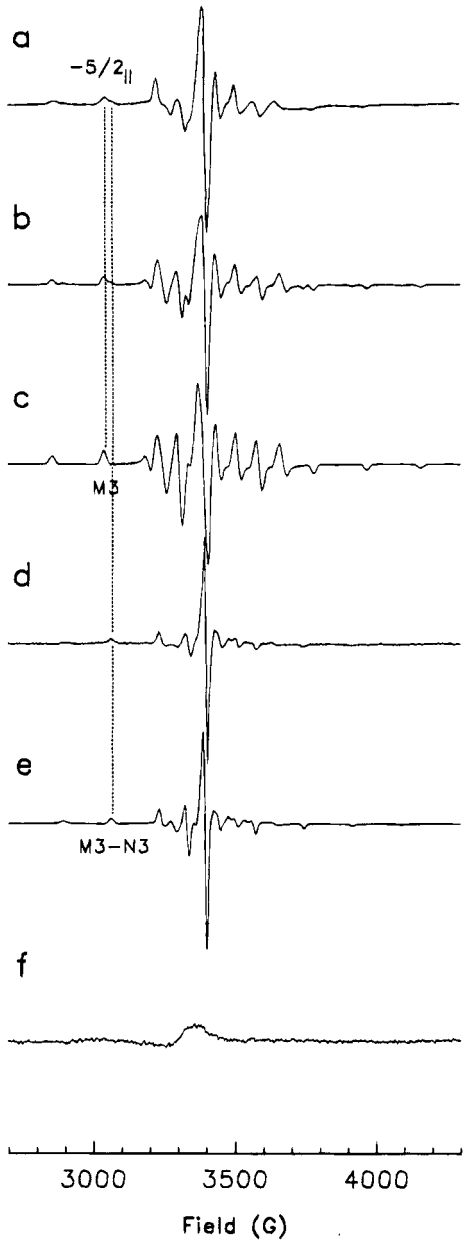

FIGURE 2: EPR spectra from VO^{2+} bound to the M3 site of CF_1 after the M2−N2 site is filled with Mg^{2+}-ATP and M3 is depleted by size-exclusion chromatography. A 1.3:1 ADP:VO^{2+} ratio was used to add 0.67 equiv of VO^{2+} of CF_1 at a concentration of 18.7 mg of CF_1 in 0.19 mL. (a) Experimental spectrum of the VO^{2+} bound to the latent CF_1 obtained with EPR conditions as in Figure 1 except 9.5547 GHz, 1.0-mW microwave power, and 82-ms time constant. (b) Simulation of (a) using a weighted sum of spectra; spectra from (e) and (f) were normalized to the same area under the $-5/2_{||}$ line and then added in the ratio of 3:1. (c) Simulation of the M3 species using the spin Hamiltonian parameters listed in Table 1 and line-width parameters W = [32, 32, 28] MHz, C_1 = [6.5, 6.5, 5.0] MHz, $C_2 = 0$, and $\epsilon = 0$. (d) Experimental spectrum of CF_1 activated with 50 mM DTT for 18 h which shows only the M3−N3 species. The sample contained 18.7 mg of CF_1 with 0.19 mM VO^{2+} and ADP in a 1:1 ratio. EPR conditions as in (a). (e) Simulation of (d) using the spin Hamiltonian parameters in Table 1 and the line-width parameters W = [17, 18, 18] MHz, C_1 = [10, 11, 9] MHz, $C_2 = 0$, and $\epsilon = 0$. (f) Control sample for (d) containing the same concentrations of DTT and VO^{2+}−ADP in 50 mM HEPES buffer without CF_1. EPR conditions as in (d).

mnd-CF_1 with VO^{2+} and ADP in this manner results in a mixed population of enzyme containing the M3 and M3−N3 species in approximately these relative proportions. Some variability in these ratios was observed from sample

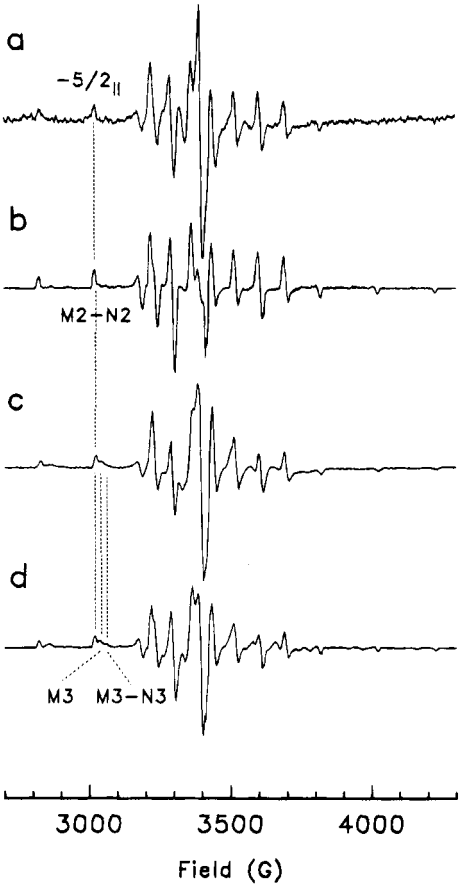

FIGURE 3: (a) Experimental EPR spectrum of the M2−N2 species alone using 40 mg of CF_1 in 350 μL; CF_1 was preloaded with VO^{2+}-ATP at the M2−N2 site as in Figure 1 followed by gel filtration chromatography to remove all VO^{2+}-ATP not bound at M2−N2. (b) Simulation of (a) with the spin Hamiltonian parameters listed in Table 1 and line-width parameters W = [20, 20, 7.8] MHz, C_1 = [2, 2, 2] MHz, $C_2 = 0$, $\epsilon = 0$. Simulation also included ^{31}P superhyperfine coupling of A = [18, 18, 18] MHz. (c) Experimental EPR spectrum of mnd-CF_1 in the presence of VO^{2+} and ATP showing the M2−N2, M3, and M3−N3 species. Conditions as in Figure 1 except 1-mW microwave power. (d) Simulation of (c) as the sum of Figure 2c,e and (b). The simulation was normalized to the same area under the $-5/2_{||}$ features and then weighted in the ratio 5:3:1 before summation. The three species M2−N2, M3, and M3−N3 are denoted in the figure at the $-5/2_{||}$ region.

to sample, however. Though samples rarely had a greater proportion of the M3−N3 species than that shown here, the abundance of this species was observed to be as low as 10% of the total metal bound to site 3 in latent CF_1.

The experimental and simulated spectra of the monodentate VO^{2+}−ATP complex at the M2−N2 site are shown in curves a and b of Figure 3, respectively. The experimental spectrum arises from bound VO^{2+} and ATP after the sample of Figure 1 was depleted of metal and nucleotide from sites with lower affinity (primarily M3 and M3−N3) by extensive gel filtration chromatography. At each parallel feature of the EPR spectrum (e.g., $-5/2_{||}$, Figure 1), the equatorial monodentate coordination of ATP to this complex gives rise to a 1:1 doublet from ^{31}P superhyperfine coupling with A_{obs} = 6.6 G or 18 MHz (Houseman et al., 1994b). As shown in Table 1, this species of bound VO^{2+} has much larger ^{51}V hyperfine couplings and much smaller g values than those observed for VO^{2+} bound alone at the M2 or M3 sites.

As shown in Figure 3a, gel filtration removed all contributions of VO^{2+} bound to the M3 site. Contributions of the

M3−N3 species are also not evident in the $-5/2_{||}$ line, apparently leaving only the M2−N2 species. However, comparison of the $-1/2_{||,\perp}$ line of the experimental and simulated spectra of the M2−N2 species reveals that it is impossible to simulate both the central peak and the other features of this experimental spectrum simultaneously using the single VO^{2+} EPR powder pattern of the M2−N2 species alone. The experimental spectrum that arises from the M2−N2 species can only be completely simulated if trace amounts of the simulated spectrum from the M3−N3 are included (data not shown). Thus, trace amounts of VO^{2+} bound as the M3−N3 species under these conditions must remain after chromatography that contribute significant intensity to the central peak but little intensity to the other features.

Addition of VO^{2+} and ATP to latent mnd-CF_1 results in the binding of VO^{2+} to sites 2 and 3 in the M2−N2, M3, and M3−N3 species. The entire EPR spectrum that arises from VO^{2+} bound in this manner is shown in Figure 3c (from which the $-5/2_{||}$ line is shown in details in Figure 1). The reconstruction of this spectrum obtained from the sum of the simulated spectra of site 2 (M2−N2 species) and site 3 (M3 and M3−N3 species) is shown in Figure 3d.

The line widths of the VO^{2+} spectra are relatively narrow and the barely resolved ^{31}P coupling in the M2−N2 complex is only 6.6 G in magnitude. An approximate calculation shows that the dipolar spin−spin interaction between the VO^{2+} ions will broaden the widths of the EPR lines significantly from that observed when each site is filled alone (i.e., samples shown in Figures 2a,d and 3a) if the M2 and M3 sites are within about 16 Å of each other (Abragam & Bleaney, 1970). Reconstruction of the spectrum 3c in Figure 3d was possible merely by normalizing the area under the $-5/2_{||}$ features and then summing the intensity of the M2−N2, M3, and M3−N3 species as a 5:3:1 ratio. Since no additional line broadening was required to reconstruct this spectrum, it is unlikely that the metals bound at site 2 and site 3 are within 16 Å of each other. This is also supported by the observation that the $-5/2_{||}$ line of the M2−N2 species alone (Figure 3a) and that of the three species together (Figure 3c) could be fit to the same Gaussian line shape (data not shown), indicating that the presence of VO^{2+} in site 3 does not broaden the EPR signal that arises from the M2−N2 species.

The ^{51}V hyperfine couplings for the three species of VO^{2+} bound to CF_1 shown in Table 1 can be estimated using the additivity relation of eq 1 (Chasteen, 1981) since the **g** and **A** tensors are approximately a linear combination of tensors from each type of group that contributes an equatorial ligand to the metal (Holyk, 1979; Chasteen, 1981; Markham, 1984). These results can provide information concerning the combination of equatorial ligands to the bound VO^{2+}, particularly if independent evidence of the identity of one or more of the ligands exists.

ESEEM spectroscopy can provide a direct probe of the local environment of the VO^{2+} and is a particularly sensitive means of determining the presence of coordinated nitrogen. Three-pulse (stimulated echo) ESEEM was employed to characterize the local environments of the M2−N2, M3, and M3−N3 species of VO^{2+} bound to CF_1. These species were examined in samples in which each appeared individually, as well as in one sample which contained a mixture of all three metal-binding modes (Figure 3c). Results were reproduced several times at the same and different laboratory fields.

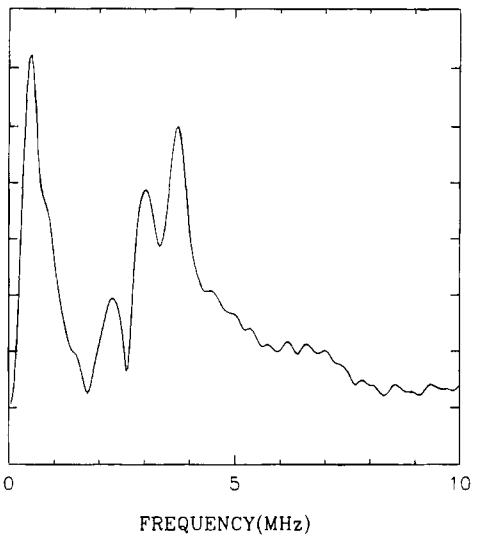

FIGURE 4: Three-pulse ESEEM of the M2−N2, M3, and M3−N3 species with 3:1 ATP:VO^{2+} whose EPR spectrum is shown in Figures 1 and 3a. Conditions: 6 K; τ, 220 ns; repetition rate, 120 Hz; microwave frequency, 8.1610 GHz. Each point is an average of 384 total repetitions. The spectrum was taken at the $-1/2_{||}$ region at 2872 G.

The ESEEM spectrum of Figure 4 originates from VO^{2+} bound to site 2 and site 3 in the presence of ATP under conditions that give rise to the CW-EPR spectrum of Figures 1 and 3c from samples that have sufficiently high CF_1 concentrations. Two resonances are evident in this spectrum at 3.2 and 3.6 MHz. We have recently found that crystallographically defined model complexes that contain an amine nitrogen ligand at the axial position have spin-echo modulations in the 3−4 MHz range, similar to the CF_1-bound VO^{2+} of Figure 4 (unpublished results). In all cases examined thus far, these resonances are only observed at significantly higher sample concentrations than are necessary to resolve the resonances at about 4 and 7 MHz that result from $\Delta m_I = \pm 2$ "double-quantum" transitions of an equatorially coordinated amine nitrogen (Zhang et al., 1993). The resonances observed with CF_1 in the 3−4 MHz range of Figure 4 are likely to originate from VO^{2+} bound to some of the CF_1 in a manner that involves a nitrogen ligand at the axial position or in the second coordination sphere.

ESEEM spectra for the VO^{2+} bound individual M2−N2, M3, and M3−N3 species were also obtained. Except for a resonance at the ^1H Larmor frequency, no spin-echo modulations were detected in any of the four samples (data not shown). This absence indicates that nitrogen from either lysine or histidine can be eliminated as a possible equatorial ligand to the VO^{2+} bound under these conditions to these sites. The absence of the modulations that are consistent with an axial nitrogen ligand from these latter samples is probably the result of the lower sample concentrations obtained as a result of isolating each of the individual species such that the size of the modulations was below the limit of detection.

DISCUSSION

Probable Ligands of the Metals Bound at Sites 2 and 3. The analysis of the EPR spectra and information obtained from the ESEEM experiments reported here provide evidence

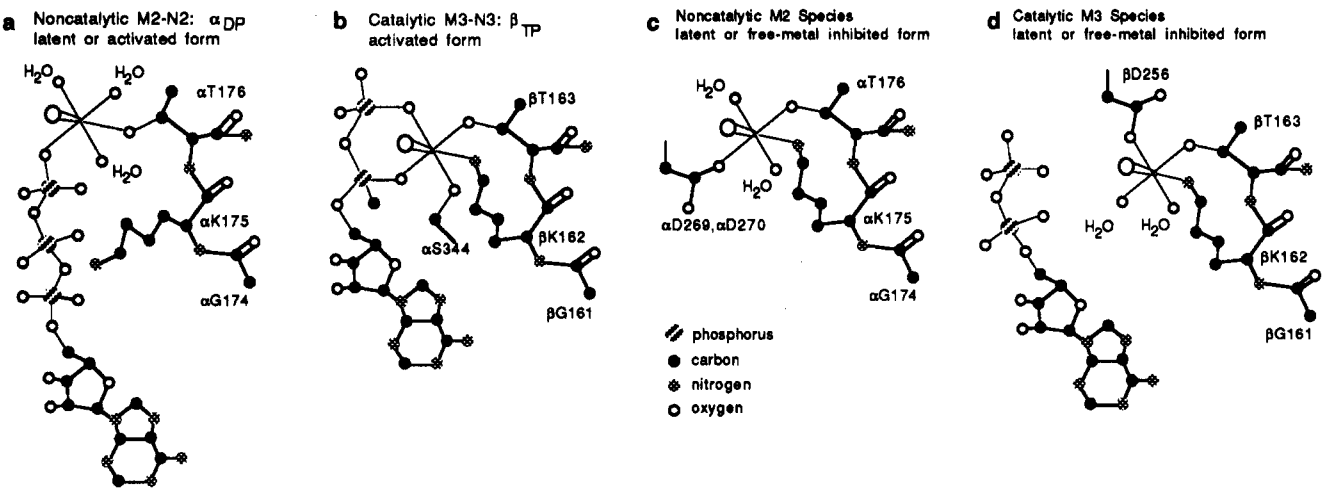

FIGURE 5: Summary of metal coordination at the M2 and M3 sites.

of probable coordination environments for the M2 and M3 metal-binding sites under three different conditions: (i) latent CF_1 without free ATP in solution, (ii) latent CF_1 with free ATP in solution, and (iii) activated CF_1. Figure 5 shows a summary of the ligands to each of these species, which are best fits of the data from Table 1, as estimated from the additivity relation given in eq 1.

In Figure 5a, CF_1 has been depleted of nucleotide in all but the N1 site, and VO^{2+} has been added in the presence of ATP to the latent enzyme to fill sites 2 and 3 predominantly as the M2−N2 and M3 species. The EPR signal of the VO^{2+}−ATP complex at the M2−N2 site shows no evidence of equatorial ^{14}N coordination from ESEEM spectroscopy. Given that a single ATP phosphate oxygen is an equatorial ligand from the doublet in the EPR spectrum with a coupling equivalent to that of ^{31}P, the VO^{2+} bound at this site has particularly large ^{51}V hyperfine values while the g values are quite small (Table 1, line 2). To our knowledge, only oxygens from water can serve as ligands at the remaining three equatorial positions of the M2−N2 monodentate metal−ATP complex and give rise to the observed values of **A** and **g** (Table 1, line 10).[2]

In relating the M3−N3 species of activated CF_1 to its ligation environment, the best fit to the data from the M3−N3 species is obtained with two hydroxyls from serine or threonine and two phosphate oxygens from the nucleotide as depicted in Figure 5b (see also Table 1, line 17). This is consistent with (i) the lack of strong ^{14}N coupling in the ESEEM spectrum of this species and (ii) evidence that suggests the presence of a bidentate VO^{2+}−ADP complex bound to site 2 under these conditions (Houseman et al., 1994b).

The evidence suggests that VO^{2+} bound at M3 lacks coordinated phosphates from the nucleotide as well as nitrogen-containing ligands. Thus, as shown in Figure 5d, the best fit of the data of VO^{2+} bound at the M3 site via the additivity relation is one hydroxyl oxygen from Ser or Thr, one carboxyl oxygen from Asp or Glu, and two water oxygens as equatorial ligands (Table 1, line 15). This is consistent with the ligand set suggested for the M3 site by Houseman et al. (1994a). In samples containing the M2 species that do not demonstrate an equatorial amine nitrogen ligand, the data are best fit by the same ligand set as that described for the M3 species (Figure 5c).

Under conditions in which the M2−N2, M3, and M3−N3 species are all present (Figures 1 and 3c), we observe ESEEM frequencies indicative of a nitrogen coordinated in the axial position of the bound VO^{2+}. In cases where nitrogen coordinates VO^{2+} equatorially, the isotropic part of the superhyperfine coupling, A_{iso}, is large relative to the nuclear Zeeman interaction. In this situation one generally observes two sharp $\Delta m_I = \pm 2$ nuclear transitions in the frequency-domain spectrum in the approximate ranges of 4−5 and 7−9 MHz (Tipton et al., 1989; Zhang et al., 1993). In contrast, when the nuclear Zeeman term is nearly equal in magnitude to $A_{iso}/2$, a spectrum containing the pure quadrupolar frequencies of the ^{14}N nucleus (plus the $\Delta m_I = \pm 2$ transition from the other electronic manifold) is seen (Mims & Peisach, 1978). Between these two extremes, ^{14}N ESEEM spectra are less well characterized. However, since the $\Delta m_I = \pm 2$ transitions must pass from below the 3−4-MHz frequency range in the second case to above that range in the first, it is natural to suspect that the observed peaks arise from a superhyperfine coupling that is intermediate between those which define the limiting cases described above. Determination of superhyperfine and nuclear quadrupole parameters represented by the spectrum of Figure 5 will be most readily obtained from detailed examination of the magnetic field dependence of the spectral lines, preferably at multiple microwave excitation frequencies, and by spectral simulations. Such a determination is beyond the scope of the present paper.

Chasteen (1981) has observed that in-plane strain on the L−V−L angle can make small, but significant, differences in ^{51}V hyperfine coupling even from nearly identical ligands (L) as in the case of the oxalate chelate ring having a 4% smaller A_{iso} than the larger malonate chelate ring. The presence of bidentate ADP in M3−N3 of CF_1 would contribute significantly to this strain. The X-band EPR spectra of the M3−N3 species do show a measurable degree of **g** and **A** rhombicity which may also be an effect of ring strain. Such rhombicity is fairly common (Chasteen, 1981),

[2] The $A_{||}$ of a crystallographically defined VO^{2+} complex that contains a carbonyl O ligand from a single amide group is consistent with a hyperfine coupling of this ligand equivalent to a water oxygen (unpublished results). More experiments are required to determine whether this ligand of this model complex is replaced by water in solution before carbonyl oxygens from Asn, Gln, or the peptide backbone can be considered as potential ligands.

and the extent of rhombicity observed here is 24% in **g** and 9% in **A**, as measured by the difference in the two "perpendicular" values divided by the difference of the parallel value and the average "perpendicular" value (see Table 1). The M2, M2−N2, and M3 species, however, displayed no detectable rhombicity.

Probable Locations of the Metal Ligands on the α and β Subunits. The 2.8 Å crystal structure of the MF_1-ATPase (Abrahams et al., 1994) provides an extensive amount of structural information concerning protein folding and the general location of the metal−nucleotide complexes on the α and β subunits. However, this structure does not resolve the relative positions of the phosphate moieties, the metals, or most of the ligands to the metals at either the catalytic or noncatalytic sites. The results presented here confirm our previous suggestion that metal bound at the catalytic sites has a hydroxylato ligand from a serine or threonine (Houseman et al., 1994a). The crystal structure also confirmed this conclusion in that the only protein ligand to metal at the catalytic sites resolved in this structure is βT163. To simplify the comparison of the residues reported here as possible ligands with their proposed positions in the crystal structure, residue assignments of the bovine mitochondrial F_1-ATPase will be designated.

The data presented here concerning the M3−N3 species in activated CF_1 are most consistent with two hydroxylato ligands. Iwamoto et al. (1993) suggested that βS174 may be coordinated to the metal at the catalytic sites based on site-directed mutagenesis studies that showed changes in metal specificity when a phenylalanine is substituted at this position. However, βS174 clearly cannot be a metal ligand since it is at least 15 Å from the metal−nucleotide binding pocket (Abrahams et al., 1994). The most likely candidate for the second hydroxyl group based on proximities to the catalytic site in the published structure is αS344, which is close to the site only in the β_{TP} catalytic site as defined by Abrahams et al. (1994).

Houseman et al. (1994b) also presented evidence that the catalytic M3−N3 species in activated CF_1 is a bidentate complex with the α- and β-phosphates of ADP or ATP. This conclusion is also confirmed by the structure of Abrahams et al. (1994), but again only in the β_{TP} catalytic site. Thus, the results presented here suggest that the M3−N3 species in activated CF_1 is the equivalent of the β_{TP} catalytic site in MF_1.

The possible identity of the M3−N3 species of CF_1 and the β_{TP} catalytic site in MF_1 has further implications for nucleotide-binding sites N1, N2, and to some extent N4 as well since the metal- and nucleotide-binding properties of these sites are known (Bruist & Hammes, 1981; Houseman et al., 1994b), and their locations have been determined relative to specific locations on the α and γ subunits using fluorescence resonance energy transfer (Richter et al., 1985). On the basis of binding specificities, the catalytic N1 site (with tightly bound Mg^{2+}-ADP) and the catalytic N4 site (the last catalytic site to fill) should correspond on MF_1 to the β_{DP} and β_E sites, respectively.

Using 2′-*O*-tetranitrophenyl-ATP (TNP-ATP) as a fluorescent probe, the distance between the N1 and N3 sites was measured to be about 48 Å (Richter et al., 1985; Shapiro et al., 1991), which is quite comparable to the distances between the catalytic sites in the structure of Abrahams et al. (1994). At first inspection, the N1−N2 and the N3−N2 distances, 43 and 36 Å, respectively (Shapiro et al., 1991), do not correspond to the distances between the catalytic sites or any of the three noncatalytic sites which are on average 27 Å from adjacent catalytic sites (Abrahams et al., 1994). However, a rough estimation of the distance and orientation of the TNP groups relative to the ribose of the nucleotides bound at the β_{DP}, α_{DP}, and β_{TP} sites can account for distances of about 39 Å (versus 43 Å) and 32 Å (versus 36 Å) between $\beta_{DP}-\alpha_{DP}$ and $\beta_{TP}-\alpha_{DP}$, respectively. The distances and orientations of N1, N2, and N3 on CF_1 relative to the lucifer yellow site (αK384) and particularly the S3 site (the light NEM-modifiable site, γC78) are all consistent with β_{DP}, α_{DP}, and β_{TP}, respectively, in support of our data.

The lack of broadening of the EPR signals from the VO^{2+} bound at the M2 or M3 sites reported here when both sites are filled indicates that the metals associated with these adjacent catalytic and noncatalytic sites are at least 16 Å apart in the spinach chloroplast F_1-ATPase. With a distance of about 27 Å between β-phosphates of the nucleotides at the adjacent α_{DP} and β_{TP} sites in the Abrahams et al. (1994) structure, our results suggest that the distance and orientation of adjacent catalytic and noncatlytic metal−nucleotide complexes in CF_1 are similar to the crystal structure.

To date, we have been unable to determine which, if not all, of the species has an axial N ligand from an amine, since the sample concentrations of each of the isolated species presented here are below the threshold of detectability of an axial nitrogen ligand. Given that βT163 is an equatorial metal ligand to VO^{2+} at the catalytic site, the bidentate metal−nucleotide complex would constrain the binding orientation of VO^{2+} such that its axial ligand is facing βK162, strongly implicating this group.

The data presented here are consistent with three water oxygens and one phosphate oxygen from ATP as the equatorial ligands to the vanadyl bound at the M2−N2 site.[3] Abrahams et al. (1994) report that αT176 remains a ligand to the metal at the α_{DP} site. If correct, αT176 must be an axial ligand to VO^{2+} which would not be detectable by our experiments. If the M2−N2 species is the α_{DP} site as suggested here, αT176 would provide a tether to the metal−nucleotide complex in addition to the βY368 which binds the adenine ring only in the α_{DP} form.

We have previously shown (Houseman et al., 1994b) that the M2−N2 species is a monodentate metal−ATP complex such that only one phosphate oxygen of ATP is equatorially coordinated to the metal in this form, which is likely the α_{DP} site in the structure of Abrahams et al. (1994). Though these researchers report that only the γ-phosphate of ATP is coordinated to the metal, they conclude that two of the oxygens of this phosphate are ligands. The data presented here indicate that in our studies with VO^{2+} this is not the case for the following reasons. First, the additivity relation indicates that only one phosphate oxygen is coordinated equatorially such that, if a second phosphate oxygen is a metal ligand, it must be an axial ligand to the VO^{2+} under these conditions, but the axial ligand has already been suggested to be αT176 at the α_{DP} site as described above. Second, coordination by two oxygens of the same phosphate

[3] If a carbonyl O from an amide does prove to form a ligand in aqueous solution and gives rise to a coupling comparable to water, αQ208, the spatial equivalent to βD188 at the catalytic site, is the most probable ligand.

would create a four-membered ring between the metal and the γ-phosphate. This would create significant rhombicity, particularly if one of the oxygen ligands is an axial ligand. However, there is no evidence of rhombicity in the M2−N2 species.

The crystal structure of Abrahams et al. (1994) is unable to reveal the free-metal-inhibited state of the enzyme. At the M3 site, βT163 and βK162 remain likely candiates for metal ligands as shown in Figure 5d. The data presented here are consistent with an equatorial carboxylato ligand to the free-metal-bound form as well. One candidate for this carboxyl group is βE188 for which there are data that support (Vallejos, 1981) and oppose (Dagget et al., 1985) this group as a metal ligand. In the crystal structure, this group is positioned 4.4 Å from the γ-phosphate of the bound AMPPNP with an intervening water that makes this residue appropriately positioned to facilitate a nucleophilic attack of the water on the terminal phosphate. This fact may account for the dramatic effects on enzymatic activity observed with site-directed mutants at this site (Parsonage et al., 1988; Hu et al., 1995). If this is the function of this group, coordination of this residue by the metal in the absence of nucleotide would account for free-metal inhibition. A second candidate for this carboxyl group is βD256 since mutation of this residue prevents inhibition of ATPase activity by free metal (Senior & Al-Shawi, 1992). The absence of a carboxylato ligand in the M3−N3 species (Figure 5b) in our data may result from the inability to detect axial ligands with VO^{2+}.

The equatorial hydroxylato ligand to free metal bound at M2 is most likely to be αT176 as indicated by the structure of Abrahams et al. (1994) for metal−nucleotide bound to the noncatalytic sites. As per the discussion of the M2−N2 site above, αK175 is implicated for the axial ligand of this species as well. Carboxylato groups that could serve as possible ligands to the metal at this site include αD269 and αD270. This conclusion is based solely on their proximity to the metal in the metal−nucleotide bound structure of the noncatalytic site (Abrahams et al., 1994).

Functional Basis for the Observed Changes in Metal Ligation. In the latent enzyme, even though metal and nucleotide are bound at the catalytic site 3, the phosphate oxygens are not coordinated to the metal. However, treatments that activate CF_1 induce a conformational change that allows ADP at N3 to coordinate in a bidentate fashion to metal at M3, forming the M3−N3 species (Houseman et al., 1994b). This change is consistent with previous results which show that nucleotide phosphates at catalytic sites are coordinated to metal in the activated form (Frasch & Selman, 1982; Carmeli et al., 1986; Devlin & Grisham, 1990) but not in latent CF_1 (Carmeli et al., 1989). Results presented here show that the insertion of phosphate oxygens into the coordination sphere of the metal occurs within a relatively short time compared to the time required to obtain complete activation of ATPase activity, particularly when activated by DTT alone (Nalin & McCarty, 1984). These results suggest that the formation of the metal−nucleotide complex is a relatively early step in the complex activation process.

F_1-ATPases are known to be susceptable to inhibition by the binding of metal in the absence of nucleotide (Hochman & Carmeli, 1981; Guerrero et al., 1990; Jault & Allison, 1993). Free-metal inhibition is presumably due to protein side chains that coordinate to the metal in a manner that results in nonproductive metal binding. It is noteworthy that in the absence of nucleotide the metal ligands at the catalytic M3 site (i.e., those that should cause free-metal inhibition) are approximately those of the metal binding in the presence of nucleotide when the enzyme is latent. This similarity implies that the latent state of the enzyme may result from free-metal inhibition forced by conformational change. The data also suggest that activation of the enzyme leads to the displacement of a carboxylato ligand from the metal at the catalytic site by a hydroxyl group of a second Ser or Thr. Thus, this carboxyl group is likely to compete with the phosphate oxygens for metal coordination and may be responsible for the nonproductive binding of the latent or free-metal-inhibited state.

Interconversion between ADP + P_i and ATP at the catalytic site of CF_1 has been found to involve the coordination of the α-phosphate of the nucleotide as determined by several methods (Frasch & Selman, 1981; Carmeli et al., 1989; Devlin & Grisham, 1990). The requirement for a tridentate metal−ATP complex for the reversible synthesis/hydrolysis reaction has also been observed in creatine kinase (Reed & Leyh, 1980). However, the β_{TP} form of the catalytic site of the structure of Abrahams et al. (1994) concurs with results presented here for the M3−N3 catalytic site of activated CF_1 that a bidentate metal−ATP complex is bound in this form.

A possible explanation for this apparent discrepency can be found in the binding-change hypothesis where release of product is the energy-requiring step in ATP synthesis and is induced by the binding of substrate at another catlaytic site (Boyer, 1993). According to this hypothesis, one catalytic site contains bound ATP (putatively β_{TP}) while a second is in a conformation that allows rapid interchange between ADP + P_i and ATP (putatively β_{DP}). Binding of ADP and phosphate to the third, empty site then allows the protonmotive-force-induced conformational changes to occur that release the ATP from β_{TP} and slow the hydrolysis reaction of the rapidly interconverting catalytic site (i.e., convert β_{DP} to β_{TP}).

The dissociation constants of exchange-inert bidentate Cr-ATP and tridentate Cr-ATP at the catalytic sites of CF_1 have been determined to be 724 and 186 mM, respectively (Frasch & Selman, 1992). If the β_{DP} is converted to the β_{TP} form via the binding-change mechanism, this conformational change would include the insertion of αS344 into the catalytic site since this residue is present only in the β_{TP} form. Results presented here show the presence of a second hydroxyl group as a ligand under these conditions which is possibly αS344. Insertion of αS344 into the coordination sphere of the metal upon formation of the β_{TP} form could convert the tightly bound tridentate metal−ATP complex to a bidentate metal−ATP complex where dissociation of ATP from the enzyme would then be favored over its subsequent hydrolysis. In the event that αS344 displaces the α-phosphate when β-$_{DP}$ contains ADP, the resulting monodentate metal−ADP complex is not likely to dissociate since the K_D of monodentate Cr-ADP is 17 μM (Frasch & Selman, 1982). This provides a gating mechanism such that harnessing the protonmotive force to release nucleotide favors release of ATP over ADP even against an unfavorable ATP/ADP concentration gradient. However, neither the structure of Abrahams et al. (1994) nor the data presented here provide evidence that catalytic events cause the interconversion of

the different conformation of the nucleotide-binding sites. EPR experiments are currently underway to describe the changes at these sites that result from single and multiple catalytic events.

The presence of hydroxylato ligands from serines and threonines is not unique to the F_1-ATPase but has also been observed at the Mg^{2+}-binding sites of $p21^{H-ras}$ (Pai et al., 1989) and myosin (Digel et al., 1994). In both cases, the first hydroxylato ligand originates from the GXXXXGKT/S sequence while the second is on a separate domain of the protein. In $p21^{H-ras}$, these groups affect the ability of the enzyme to bind and hydrolyze the nucleotide (John et al., 1993). This is mediated in part by the second hydroxyl-containing residue which is a ligand to the Mg^{2+}−GTP complex but not the Mg^{2+}−GDP complex. Comparison to the results presented here suggests a common means by which enzymes use the binding metal−nucleotide complexes to drive chemomechanical changes and may provide insight into the basis for the metal−nucleotide requirement of a wide variety of enzymes including myosin, the nitrogenase iron protein, the cystic fibrosis translocating regulator, and chaperonins among others.

REFERENCES

Abragam, A., & Bleaney, B. (1970) in *Electron Paramagnetic Resonance of Transition Ions*, Oxford University Press, Oxford, UK.

Abrahams, J. P., Leslie, A. G. W., Lutter, R., & Walker, J. E. (1994) *Nature 370*, 621−628.

Albanese, N. F., & Chasteen, N. D. (1978a) *J. Phys. Chem. 82*, 910−914.

Albanese, N. F., & Chasteen, N. D. (1978b) *J. Phys. Chem. 82*, 2758.

Boyer, P. D. (1993) *Biochim. Biophys. Acta 1140*, 215−250.

Bruist, M. F., & Hammes, G. G. (1981) *Biochemistry 20*, 6298−6305.

Carmeli, C., Huang, J., Mills, D., Jagendorf, A., & Lewis, A. (1986) *J. Biol. Chem. 261*, 14171−14177.

Carmeli, C., Lewis, A., & Jagendorf, A. T. (1989) in *Current Research in Photosynthesis* (Baltscheffsky, M., Ed.) Vol. III, pp 29−32, Kluwer, Dordrecht, The Netherlands.

Chasteen, N. D. (1981) in *Biological Magnetic Resonance* (Berliner, L., & Reuben, J., Eds.) pp 53−119, Plenum Press, New York.

Dagget, S. G., Gruys, K. J., & Schuster, S. M. (1985) *J. Biol. Chem. 260*, 6213−6218.

Devlin, C., & Grisham, C. (1990) *Biochemistry 29*, 6192−6203.

Digel, J., LoBrutto, R., Rayment, I., Smith, R., Laughlin, L. T., & Reed, G. H. (1994) *Abstracts of the 36th Rocky Mountain Conference on Analytical Chemistry*, Denver, CO, No. 144.

Frasch, W. D. (1994) in *Photosynthesis of the Cyanobacteria* (Briant, D. A., Ed.) Chapter 11, pp 361−380, Kluwer Academic Publishers, Dordrecht, The Netherlands.

Frasch, W. D., & Selman, B. R. (1982) *Biochemistry 21*, 3636−3643.

Froncisz, W., & Hyde, J. S. (1980) *J. Chem. Phys. 73*, 3123−3131.

Guerrero, K. J., Xue, Z., & Boyer, P. D. (1990) *J. Biol. Chem. 265*, 16280−16287.

Haddy, A. E., Frasch, W. D., & Sharp, R. R. (1985) *Biochemistry 24*, 7926−7930.

Hochman, Y., & Carmeli, C. (1981) *Biochemistry 20*, 6287−6292.

Holyk, N. (1979) M.S. Thesis, University of New Hampshire, Durham, NH.

Houseman, A. L. P., Morgan, L., LoBrutto, R., & Frasch, W. (1994a) *Biochemistry 33*, 4910−4917.

Houseman, A. L. P., LoBrutto, R., & Frasch, W. (1994b) *Biochemistry 33*, 10000−10006.

Hu, C.-Y., Morgan, L., Webber, A., & Frasch, W. D. (1995) (submitted for publication).

Iwamoto, A., Park, M.-Y., Maeda, M., & Futai, M. (1993) *J. Biol. Chem. 268*, 3156−3160.

Jault, J.-M., & Allison, W. S. (1993) *J. Biol. Chem. 268*, 1558−1566.

John, J., Rensland, H., Schlichting, I., Vetter, I., Borasio, G. D., Goody, R. S., & Wittinghofer, A. (1993) *J. Biol. Chem. 268*, 923−929.

LoBrutto, R., Smithers, G. W., Reed, G. H., Orme-Johnson, W., Tan, S. L., & Leigh, J. S. (1986) *Biochemistry 25*, 5654−5660.

Markham, G. D. (1984) *Biochemistry 23*, 471−478.

Maurice, A. M. (1980) Ph.D. Thesis, University of Illinois, Urbana, IL.

Mims, W. B., & Peisach, J. (1978) *J. Chem. Phys. 69*, 4921−4930.

Nalin, C. M., & McCarty, R. E. (1984) *J. Biol. Chem. 259*, 7275−7280.

Nilges, M. J. (1979) Ph.D. Thesis, University of Illinois, Urbana, IL.

Pai, E., Kabsch, W., Krengel, U., Holmes, K. C., John, J., & Wittinghofer, A. (1989) *Nature 341*, 209−214.

Parsonage, D., Wilke-Mounts, S., & Senior, A. (1988) *FEBS Lett. 233*, 111−114.

Reed, G. H., & Leyh, J. S. (1980) *Biochemistry 19*, 5472−5480.

Reijerse, E. J., Shane, J., de Boer, E., & Collison, D. (1989) in *Electron Magnetic Resonance of Disordered Systems* (Yordanov, N. D., Ed.) pp 189−204, World Scientific Publishers, London.

Richter, M. L., Snyder, B., McCarty, R. E., & Hammes, G. G. (1985) *Biochemistry 24*, 5755−5763.

Senior, A. E., & Al-Shawi, M. K. (1992) *J. Biol. Chem. 267*, 21471−21478.

Shapiro, A. B., Huber, A. H., & McCarty, R. E. (1991) *J. Biol. Chem. 266*, 4194−4200.

Strotmann, H., Hesse, H., & Edelmann, K. (1973) *Biochim. Biophys. Acta 314*, 202−210.

Tipton, P. A., McCracken, J., Cornelius, J. B., & Peisach, J. (1989) *Biochemistry 28*, 5720−5728.

Vallejos, R. (1981) in *Energy Coupling in Photosynthesis* (Selman, B., & Selman-Reimer, S., Eds.) pp 129−139, Elsevier, North Holland.

Zhang, C., Markham, G. D., & LoBrutto, R. (1993) *Biochemistry 32*, 9866−9873.

BI942822C